




 Cite this: *RSC Adv.*, 2023, **13**, 26574

# Phototransformation of extracellular polymeric substances in activated sludge and their interaction with microplastics†

 Shuyin Wei, Feng Zeng,  Yingyue Zhou, Jiawei Zhao, Hao Wang, Rui Gao and Weiqian Liang \*

Substantial amounts of extracellular polymeric substances (EPS) are present in sludge from wastewater treatment plants (WWTP), and EPS can significantly affect the fate, bioavailability, and toxicity of microplastics (MPs) that coexist in the effluent, however, the mechanism of action between EPS and microplastics remains unclear. In addition, ultraviolet (UV) disinfection is indispensable in the wastewater treatment process in WWTP, which can significantly affect the characteristics of EPS. Therefore, it is of great significance to study the photochemical characteristics of EPS and the effect on binding MPs. In this study, using multispectral technology and two-dimensional correlation spectroscopy analysis, indicates that the molecular weight and aromaticity of EPS after phototransformation were reduced. The results showed that the adsorption of EPS on PSMPs was in the order of TB-EPS > LB-EPS > S-EPS, which was positively correlated with the SUVA<sub>254</sub>, but negatively correlated with O/C of EPS. This indicates that the main adsorption mechanisms of PSMPs on EPS were  $\pi$ - $\pi$  and hydrophobicity. The adsorption capacity of S-EPS, LB-EPS and TB-EPS to PSMPs decreased with the increasing of illumination time. After phototransformation, the adsorption sensitivity and reaction sequence of EPS and PSMPs did not change much. This research provides a theoretical basis for understanding the photochemical transformation of extracellular polymers and the morphology and migration of microplastics in sewage treatment, and evaluating the impact of microplastics on ecosystems.

 Received 15th June 2023  
 Accepted 1st September 2023

DOI: 10.1039/d3ra04027e

[rsc.li/rsc-advances](http://rsc.li/rsc-advances)

## 1. Introduction

Extracellular polymeric substances (EPS) are high molecular weight polymers produced by microorganisms and present in individuals or microbial communities, such as pure cultures, activated sludge, granular sludge, and biofilms.<sup>1</sup> EPS is composed of polysaccharides (PS), proteins (PN), humic acid (HA), fulvic acid (FA) and so on.<sup>2-4</sup> EPS composition depends on the degree of connection to the surface of the cell and can be distinguished into soluble EPS (S-EPS) and loosely bound EPS (LB-EPS) and tightly bound EPS (TB-EPS).<sup>5-7</sup> EPS in sludge has many different properties, such as hydrophilic/hydrophobic,<sup>8</sup> biosorbent sludge bioflocculation,<sup>9</sup> sludge sedimentation,<sup>10</sup> redox performance<sup>11</sup> and biodegradability,<sup>12</sup> stability.<sup>13</sup> Most of the work conducted has not considered the influence of ultraviolet light on the performance of EPS, and that ultraviolet (UV) disinfection is indispensable in the treatment process in wastewater treatment plants (WWTP),<sup>14</sup> so it is of great significance to study the phototransformation of EPS.<sup>15</sup>

Microplastics (MPs) have received widespread attention as a new type of pollutant in recent years, and it was showed that WWTP are also a key channel for microplastic pollution to enter freshwater and marine environments.<sup>16</sup> MPs adsorb EPS to form large flocs in the wastewater treatment process, increase the relative density and sedimentation rate of flocs, and facilitate the removal of microplastics in the secondary sedimentation tank.<sup>17</sup> Recently, Ye *et al.*<sup>18</sup> discovered the effect of microplastics on the physicochemical properties of extracellular polymeric substances (EPS) produced by microcystic aeruginosa. Jachimowicz *et al.*<sup>19</sup> found that polyethylene microplastics increase the production of extracellular polymeric compounds in aerobic granular sludge. Qian *et al.*<sup>20</sup> studied how polystyrene nano-plastics (PS NPs) containing different functional groups act on sludge, causing it to produce different effects of EPS properties. But the interaction mechanism between EPS and MPs is still unclear, which will affect the migration and settlement of EPS and MPs in the environment, and even hinder the development of pollutant treatment in sewage. So, it is of great value to study the adsorption of EPS on microplastics.

Based on the above questions, the purpose of this study is to extract S-EPS, LB-EPS, and TB-EPS isolated from sewage treatment plants, and to explore the photochemical transformation of EPS and its interaction with MPs as shown in Fig. 1. Polystyrene

School of Chemistry, Sun Yat-sen University, Guangzhou, 510275, China. E-mail: [liangwq3@mail2.sysu.edu.cn](mailto:liangwq3@mail2.sysu.edu.cn); [qian378378@163.com](mailto:qian378378@163.com); Tel: +8620-84114133

† Electronic supplementary information (ESI) available. See DOI: <https://doi.org/10.1039/d3ra04027e>



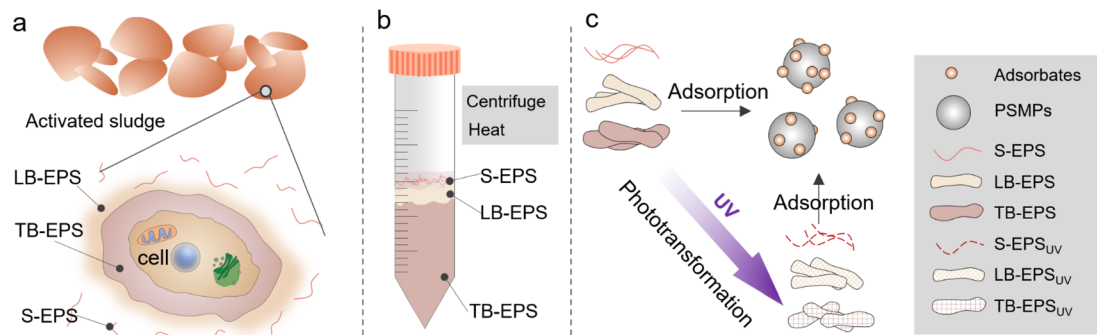


Fig. 1 Schematic illustration of EPS extraction (a and b), phototransformation and interaction with PSMPs (c).

microplastics (PSMPs) was selected as the model microplastic in this experiment. The effects of the chemical composition of PSMPs-adsorbed EPS before and after illumination were investigated by 3D-emission matrix (3D-EEM) fluorescence spectroscopy, and two-dimensional correlation spectroscopy (2D-COS) analysis. In this study, we have an in-depth understanding of the photo-dependent and adsorption heterogeneity of EPS on PSMPs, and the results are of great significance for understanding the biogeochemical behavior of EPS and MPs in wastewater treatment systems.

## 2. Materials and methods

### 2.1 Materials

PSMPs were purchased from Sigma-Aldrich (St. Aldrich, Louis, USA) and placed away from light. Activated sludge samples were taken from a municipal sewage treatment plant in Guangzhou, China, and immediately after collection, the sludge was transferred to the laboratory and stored in the refrigerator at 4 °C.

### 2.2 EPS extraction and characterization

**2.2.1 Separation of EPS.** S-EPS, LB-EPS and TB-EPS were extracted according to the heating-centrifugal extraction method, and the specific process of extraction was as follows:<sup>21</sup> 45 mL sludge samples were centrifuged at 4 °C at 8000 rpm for 5 min with the supernatant as S-EPS; resuspend the remaining sludge in the tube, add pre-heated 0.05% NaCl solution (70 °C) to dilute to the initial volume, vortex with a vortex stirrer (USA SCIOLOGEX MX-S) for 1 min, then centrifuge at 4 °C at 6000 rpm for 10 min, and the collected supernatant is LB-EPS; remaining sludge from the last step was then suspended and diluted to 45 mL, heated in a water bath at 60 °C for 30 min, then centrifuged at 6000 rpm for 15 min at 4 °C, and the collected supernatant was TB-EPS. The extracted S-EPS, LB-EPS and TB-EPS were freeze-dried at -70 °C and sealed for storage.

**2.2.2 Phototransformation experiment of EPS and characteristics analysis.** EPS solutions at 15 mg C L<sup>-1</sup> were placed in quartz tubes and irradiated with a UVA-313 lamp at an irradiance of 50 W m<sup>-2</sup> for a illumination time of 0–48 h. The temperature in the reactor was maintained at about 20 °C by cooling water. Samples with different illumination times were collected and stored at 4 °C for the next step of analysis. The EPS

after photoconversion is recorded as EPS<sub>UV</sub>, including S-EPS<sub>UV</sub>, LB-EPS<sub>UV</sub>, TB-EPS<sub>UV</sub>.

Concentrations of the EPS were quantified using a total organic carbon (TOC) analyzer (Shimadzu, Japan). The elemental compositions of the EPS were detected *via* an elemental analyzer (Elementar Analysensysteme GmbH, Germany). UV-vis absorption spectra of EPS were collected using a UV-2600 spectrophotometer (Shimadzu, Japan). Fluorescence excitation (Ex)–emission (Em) matrix (EEM) spectra of EPS were scanned using a fluorescence spectrometer (Hitachi, Japan). The SF spectra were obtained in the wavelength range of 220–550 nm with a constant offset ( $\Delta\lambda = 60$  nm), and the scan interval was 1 nm and the scan speed was 600 nm min<sup>-1</sup>.

### 2.3 Adsorption experiments of EPS onto PSMPs

The adsorption experiments were conducted with specific concentrations (15 mg C L<sup>-1</sup>) of S-EPS, LB-EPS and TB-EPS samples with pH 7.0 by adding NaOH or HCl solution (0.01 mol L<sup>-1</sup>). All adsorption experiments are performed in a dark environment to eliminate the effects of photolysis and microbial degradation on EPS. In adsorption kinetic studies, the mixtures were shaken within 12 h and subsamples were collected at specified time intervals. In isothermal adsorption studies, PSMPs (200 mg C L<sup>-1</sup>) are poured into Erlenmeyer flasks (50 mL) containing a specific concentration of EPS, and the mixed solution was continuously shaken for 6 h.

After adsorption, the mixture is microfiltered through a 0.45  $\mu$ m aqueous filtration membrane. The adsorption amount was quantified by determining the difference between the dissolved organic carbon (DOC), ultraviolet and visible spectrum (UV-vis) and fluorescence spectra of the residual solution. The precipitates are freeze-dried, infrared determination and mechanism analysis are performed.

### 2.4 Data analysis

2D-COS analysis for the SF spectral data was performed using the 2D Shige software (2D-Shigeversion 1.3, <https://sites.google.com/site/Shigemorita/home/2dshige>) to further explore the sites and sequential orders for the interaction of EPS with PSMPs. The graphs were further plotted by use of Origin 9.0 software. More information was summarized in the ESI data.†



### 3. Results and discussion

#### 3.1 Characterization of EPSs before and after phototransformation

The elemental analysis of S-EPS, LB-EPS, TB-EPS which obtained from activated sludge separation is shown in Table 1. The relative content of elements varied across the different layers of EPS: for O/C, S-EPS > LB-EPS > TB-EPS; for H/C, TB-EPS > LB-EPS > S-EPS, indicating that S-EPS contains high levels of carboxyl groups and phenolic hydroxyl groups. The order of SUVA<sub>254</sub> is TB-EPS > LB-EPS > S-EPS (Table 2), which shows TB-EPS contains more aromatic structures.<sup>22</sup> The H/C increases and O/C decreases of EPS after phototransformation, and resulting in high saturation and low aromatic conversion which are consistent with the results of Zhou *et al.*<sup>15</sup>

The FTIR spectra of S-EPS, LB-EPS and TB-EPS in activated sludge were shown in Fig. S1.† The peak 3400 cm<sup>-1</sup> indicates the presence of O–H bonds in polysaccharides, proteins, and HA,<sup>23</sup> 2919 cm<sup>-1</sup> indicates the stretching vibration of C–H bonds, which also indicates the presence of fatty bonds in polysaccharides, proteins, and HA.<sup>24</sup> The peak at 1622 cm<sup>-1</sup> indicates a C=O bond stretching vibration, associated with an amide bond, indicating the presence of a protein.<sup>23,25</sup> 1424 cm<sup>-1</sup> indicates the C=O symmetric stretch in the –COO– group, which may be related to amino acids and sugars of the protein,<sup>25,26</sup> 1123 cm<sup>-1</sup> indicates the C–OH bond vibration, 1072 cm<sup>-1</sup> indicates the presence of polysaccharide substances,<sup>27,28</sup> 996 cm<sup>-1</sup> indicates the asymmetric ester O–P–O stretch pattern of nucleic acids. The peak of COO–, C–OH with significant difference of S-EPS > LB-EPS > TB-EPS, the results are similar to the study by Yan *et al.*<sup>29</sup>

The 3D-EEM spectra (Fig. 2) show that there are three distinct peaks<sup>20</sup> in the S-EPS, peak A (Ex/Em = 275–300 nm/325–375 nm) for protein-like fractions, peak B (Ex/Em = 300–350 nm/400–460 nm) for humic-like fractions, and peak C (Ex/Em = 275–300 nm/400–460 nm) for fulvic-like fractions. LB-EPS has two significant peaks, peak B (Ex/Em = 325–375 nm/400–460 nm) for humic-like fractions, and peak C (Ex/Em = 275–300 nm/400–460 nm) for fulvic-like fractions. There are three significant peaks in TB-EPS, peak A (Ex/Em = 260–300 nm/325–375 nm) is higher than other components, peak B (Ex/Em = 300–350 nm/400–460 nm) represents humic-like fractions, and peak C (Ex/Em = 275–300 nm/400–460 nm)

Table 1 Atomic ratio of EPS before and after phototransformation

EPS	Elemental ratio		Polarity index (O + N)/C
	H/C	O/C	
S-EPS	1.71	0.731	0.910
S-EPS <sub>UV</sub>	1.84	0.623	0.722
LB-EPS	1.73	0.690	0.802
LB-EPS <sub>UV</sub>	1.75	0.602	0.714
TB-EPS	1.77	0.572	0.670
TB-EPS <sub>UV</sub>	1.90	0.483	0.581

Table 2 Spectral parameters of EPS before and after phototransformation

EPS	E <sub>2</sub> /E <sub>3</sub>	E <sub>4</sub> /E <sub>6</sub>	SUVA <sub>254</sub> (L mg C <sup>-1</sup> m <sup>-1</sup> )
S-EPS	2.75	6.84	0.373
S-EPS <sub>UV</sub>	3.88	1.62	0.0385
LB-EPS	2.64	5.12	0.481
LB-EPS <sub>UV</sub>	3.68	2.13	0.0886
TB-EPS	2.59	4.83	0.784
TB-EPS <sub>UV</sub>	3.49	1.03	0.125

represents fulvic-like fractions. After phototransformation, the protein components were significantly degraded, and humic-like fractions and fulvic-like fractions also decreased.

In the synchronous fluorescence spectrogram (Fig. S2†), three fluorescence regions can be divided according to wavelengths of 280–360 nm, 360–440 nm and 440–600 nm, corresponding to protein-like fractions, fulvic-like fractions and humic-like fractions.<sup>30–32</sup> It can be seen that the synchronous fluorescence peaks of the three EPS are different, the content of TB-EPS protein-like fractions is significantly higher than that of S-EPS and LB-EPS, and the fulvic-like fractions and humic-like fractions of LB-EPS account for a relatively large proportion. With the increase of light conversion time, the fluorescence intensity of each component gradually decreased (Fig. S3†).

#### 3.2 Adsorption kinetics and isotherm

Based on DOC and UV measurements, the adsorption kinetics of the three original EPS on PSMPs under experimental conditions are shown in Fig. S4 and Table S1.† Adsorption of EPS on PSMPs mainly occurs at the initial 6.0 h, which is consistent with previous studies.<sup>33</sup> In the initial adsorption stage, EPS occupies a large number of adsorption sites of PSMPs. With the extension of contact time, most of the adsorption sites are occupied, the adsorption rate slows down, and the adsorption gradually reaches equilibrium.<sup>33</sup> Therefore, setting the adsorption equilibrium time to 6 h can satisfy the adsorption of EPS.

The isothermal adsorption curve revealed the adsorption capacity of EPS increased with the increase of equilibrium concentration (Fig. 3). The adsorption capacity was quantitatively analyzed by Langmuir isotherm and Freundlich isotherm, and the results showed that both isotherm models could better characterize the adsorption process (Table S2†). In the Langmuir model, TB-EPS exhibited a high adsorption capacity (1.87 mg C L<sup>-1</sup>), followed by LB-EPS (1.51 mg C L<sup>-1</sup>), and the smallest by S-EPS (1.38 mg C L<sup>-1</sup>), indicating that the binding capacity of the three types of EPS to PSMPs are different.

The higher *R*<sup>2</sup> values of Freundlich model than Langmuir model suggested that Freundlich model could be better employed for characterizing equilibrium adsorption of EPS with/without illumination on PSMPs. Before illumination, the *K<sub>F</sub>* values of EPS were sorted as TB-EPS (1.23) > LB-EPS (0.835) > S-EPS (0.483). After illumination, the *K<sub>F</sub>* values of EPS were sorted as TB-EPS (0.313) > LB-EPS (0.229) > S-EPS (0.146), indicating that the adsorption capacity was TB-EPS > LB-EPS > S-



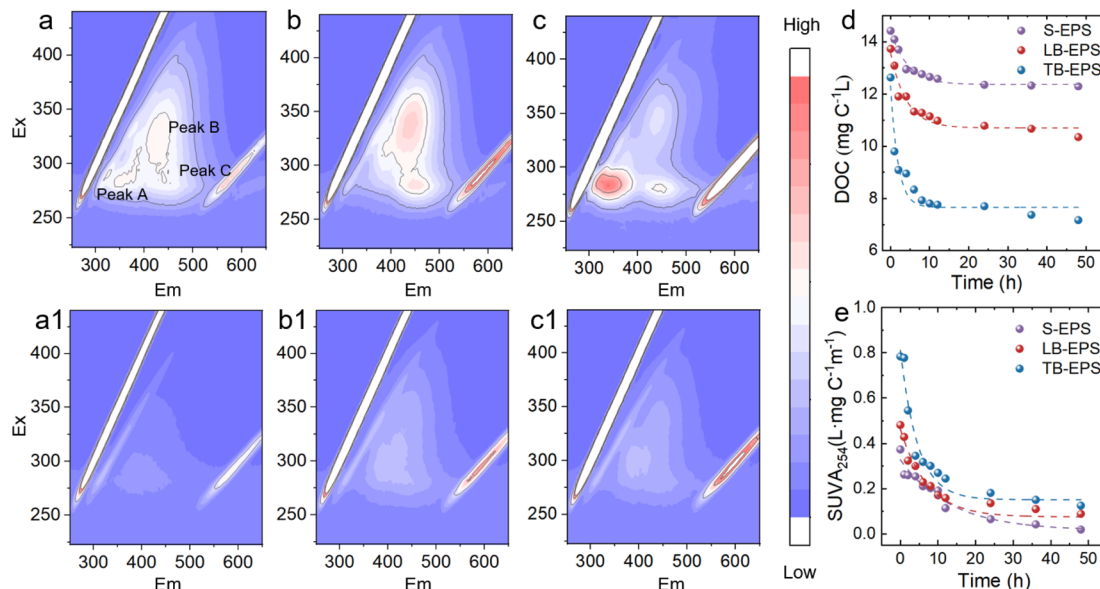


Fig. 2 Three-dimensional fluorescence of (a) S-EPS, (a1) S-EPS<sub>UV</sub>, (b) LB-EPS (b1) LB-EPS<sub>UV</sub> (c) TB-EPS (c1) TB-EPS<sub>UV</sub>; (d) TOC (e) SUVA<sub>254</sub> during phototransformation.

EPS. This may be because TB-EPS has higher aromaticity than LB-EPS and S-EPS, and hydrophobic interactions and  $\pi$ - $\pi$  electron donor receptor interactions play an important role in the adsorption process of EPS on PSMPs.<sup>18,34–36</sup>

At the same initial concentration, the Freundlich adsorption coefficient ( $K_F$ ) of the EPSs after phototransformation on PSMPs is significantly lower than that of original EPSs. This is because the phototransformation process reduces the aromaticity of EPS, thereby weakening the ability of EPS to bond with PSMPs.

### 3.3 Synchronous fluorescence 2D-COS analysis

**3.3.1 2D-SF-COS analysis of EPS before phototransformation.** With the addition of PSMPs, synchronous fluorescence patterns of S-EPS, LB-EPS, and TB-EPS are shown in Fig. 4. The intensity of protein-like fluorophores, fulvic-like fluorophores, and humic-like fluorophores decreases with the addition of PSMPs. In order to further investigate the binding characteristics, the 2D-COS spectrum generated from the SF were exhibited in Fig. 4. In 2D-SF-COS, the automatic peaks of

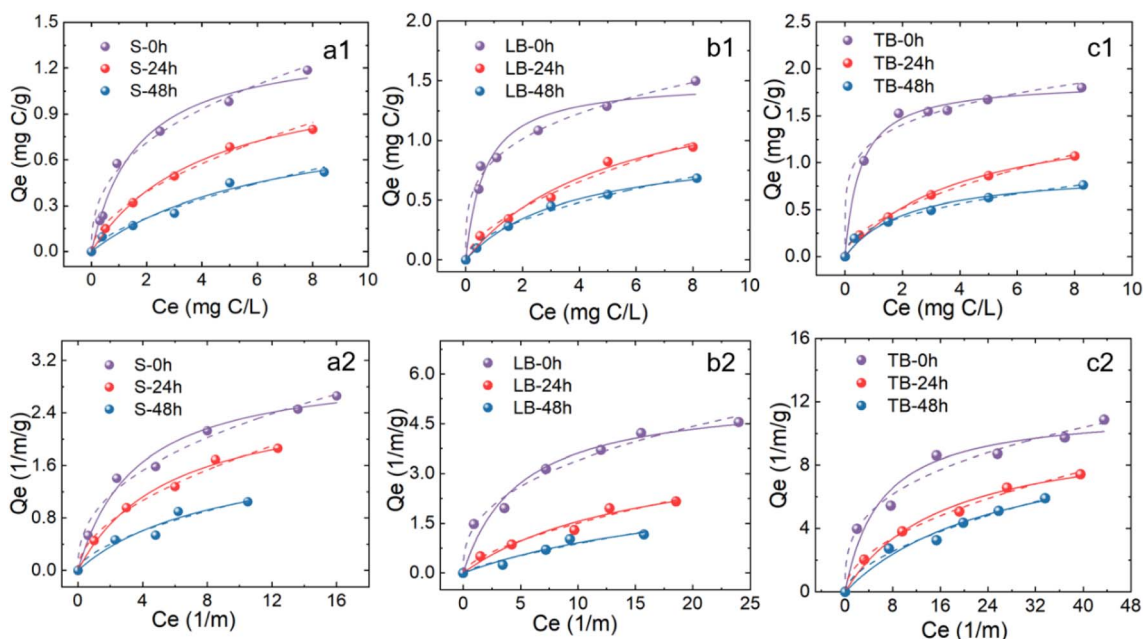


Fig. 3 Based on (a) TOC and (b) UV<sub>254</sub> analysis, the adsorption isotherm of (a1 and a2) S-EPS, (b1 and b2) LB-EPS, (c1 and c2) TB-EPS, Langmuir model (dashed line), Freundlich model (solid line) by PSMPs.



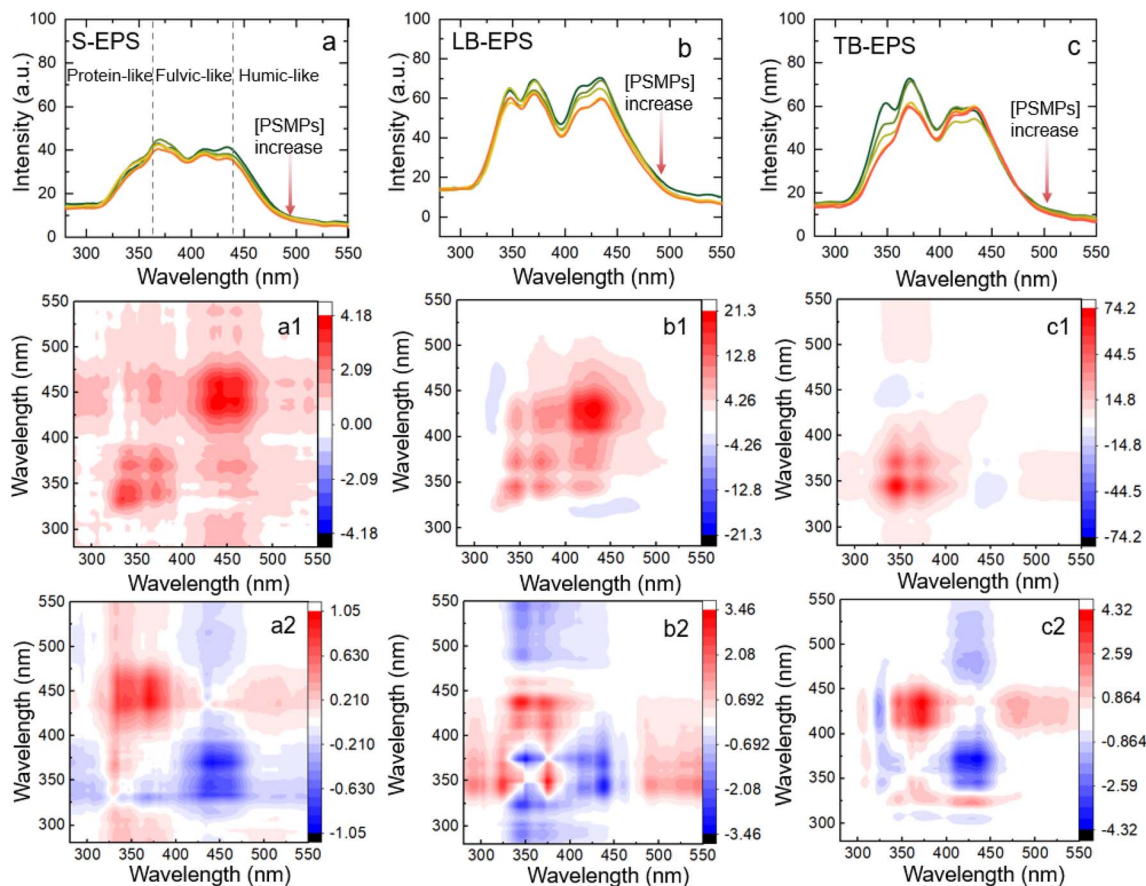


Fig. 4 Synchronous fluorescence of EPS adsorption onto PSMPs (a–c) and 2D-SF-COS diagram (a1–c1 and a2–c2).

the synchronized spectrum indicate the overall sensitivity of the corresponding spectral region to changes in spectral intensity when external perturbations are applied to the system. Cross-over peaks in asynchronous spectra detect specific sequences of spectral intensity changes by using asynchronous analysis.<sup>37,38</sup>

For S-EPS, three positively correlated peaks were observed at 340, 371, and 443 nm in synchronized spectrum (Fig. 4a1). The peak of the corresponding (340 371), (371 443) and (340 443) in asynchronous spectra is positive, indicating that protein-like substances interact with PSMPs first and then humic-like substances.

For LB-EPS, three positively correlated peaks were observed at 340, 371 and 443 nm centres in the synchronized spectrum (Fig. 4b1). It can be seen that (340 371), (371 443), and (340 443) were opposite colours in synchronized and asynchronous spectra. According to Noda's rule,<sup>39</sup> the adsorption capacity of LB-EPS on PSMPs is  $443 > 371 > 340$  nm with the increasing of PSMPs, indicating that the binding sequence with PSMPs is first humic-like fractions, then fulvic-like substances and finally protein-like fractions.

For TB-EPS, two positively correlated peaks were observed at 340 and 371 nm in synchronized spectrum (Fig. 4c1). The corresponding positive cross peaks of (320 371) and (320 443), (371 443) can be interpreted as having the same spectral change direction. According to Noda's rule,<sup>39</sup> the order of band change is  $340 > 370 > 443$  nm. The results showed that the order of

binding PSMPs was first protein-like fractions, then fulvic-like fractions and finally humic-like fractions.

**3.3.2 2D-SF-COS analysis of EPS after photo-transformation.** The synchronized fluorescence plots of S-EPS<sub>UV</sub>, LB-EPS<sub>UV</sub>, and TB-EPS<sub>UV</sub> with the addition of PSMPs are shown in Fig. 5. The intensity of the protein-like fraction, fulvic acid-like fraction and humic-like fraction decreased with increasing PSMPs. However, the degree of quenching was lower compared to the original EPSs.

The adsorption of S-EPS<sub>UV</sub> on PSMP shows two autocorrelation peaks in the synchronization plot at wavelengths of 361 and 420 nm (Fig. 5a1). In the asynchronous spectrum, (361 420), (361 443) are positive cross peaks, and (340 361) is a negative cross peak. The results showed that the binding sequences with PSMPs were first protein-like fractions, then fulvic-like fractions and finally humic-like fractions.

The adsorption of LB-EPS<sub>UV</sub> on PSMPs has two autocorrelation peaks of 340 and 410 nm in synchronized spectrum (Fig. 5b1). In the asynchronous spectrum, (340 371), (340 443) are negative cross peaks, and (371 443) are positive cross peaks, the reaction sequence is  $371 > 443 > 340$  nm. The results showed that the binding sequences with PSMPs were first humic-like fractions, then fulvic-like fractions and finally protein-like fractions, which is consistent with the high affinity of previous humic-like fractions with PSMPs.<sup>40</sup>



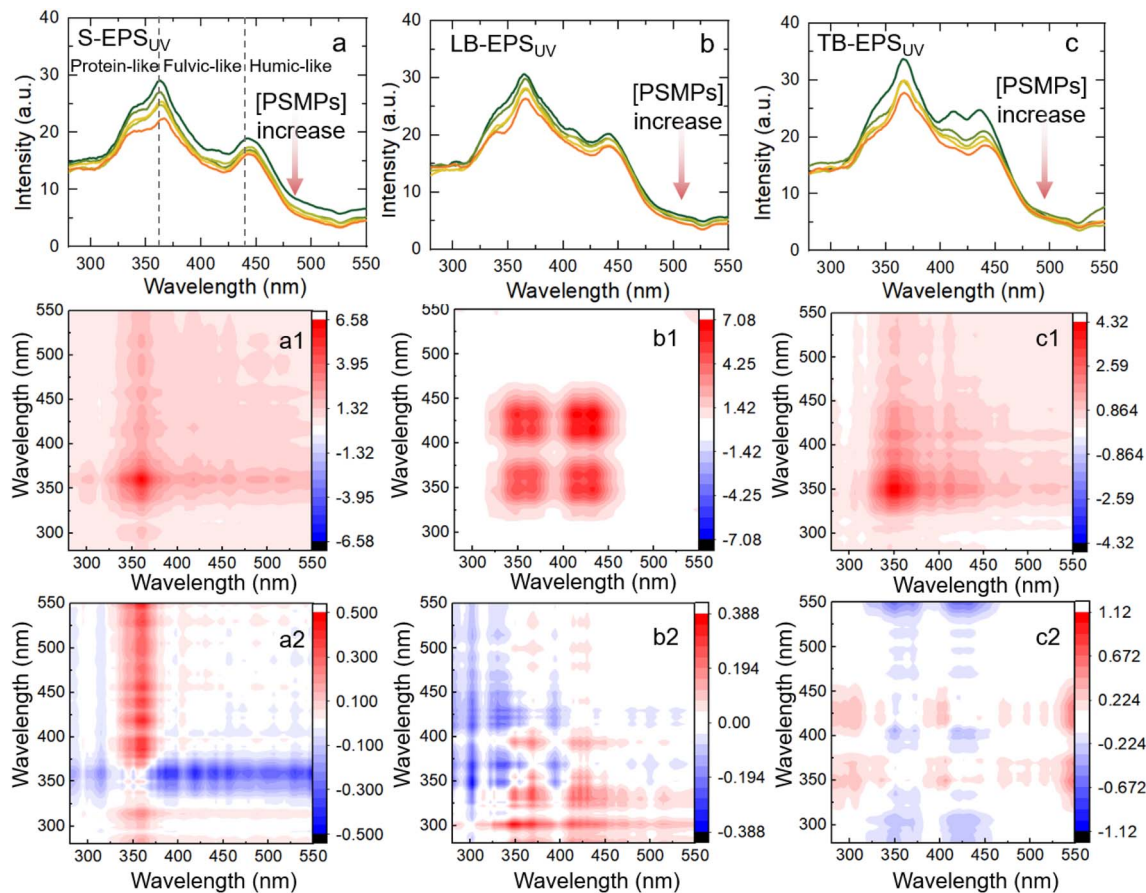


Fig. 5 Synchronous fluorescence of  $\text{EPS}_{\text{UV}}$  adsorption onto PSMPs (a–c) and 2D-SF-COS diagram (a1–c1 and a2–c2).

The adsorption of  $\text{TB-EPS}_{\text{UV}}$  on PSMPs had four related peaks of 350, 366, 410 and 434 nm in synchronized spectrum (Fig. 5c1). In addition, (330 470) as positive cross peaks and (370 470) as negative cross peaks in asynchronous spectra, indicating that the binding sequence of PSMPs was first protein-like fractions, then humus substances and finally fulvic-like fractions.

In summary, for synchronous fluorescence spectroscopy, the protein-like fractions, fulvic-like fractions and humic-like fractions of the three different layers of EPS participated in the reaction to different degrees and sequences, indicating that there was heterogeneity in adsorption. Before and after phototransformation, the protein-like components in S-EPS and TB-EPS are first involved in adsorption binding but humic-like fractions in LB-EPS, which may be due to the higher content of protein substances in S-EPS, TB-EPS, and the higher content of humic-like fractions in LB-EPS.<sup>41</sup>

## 4. Conclusions

In this study, S-EPS, LB-EPS, and TB-EPS from the sludge of WWTP were extracted and isolated, and the photochemical transformation of three types EPS and its interaction with microplastics were explored. The effects of the chemical composition of PSMPs-adsorbed EPS before and after

illumination were investigated by 3D-EEM fluorescence spectroscopy, SF, and 2D-COS analysis. The results indicate that (1) ultraviolet light significantly caused the photochemical transformation of EPS, and the molecular weight and aromaticity were reduced. (2) Compared with LB-EPS, S-EPS has higher adsorption properties, because it contains the most protein with higher aromaticity and stronger hydrophobicity, which can interact with PSMPs through  $\pi$ - $\pi$  conjugation. (3) The adsorption of PSMPs to the phototransformation of EPS was significantly reduced, because the protein, humic acid, and fulvic acid components were significantly degraded. In this study, we have an in-depth understanding of the photo-dependent and adsorption heterogeneity of EPS on PSMPs, and the results are of great significance for understanding the biogeochemical behavior of EPS and MPs in wastewater treatment systems.

In this study, the environmental behaviour of EPS and PSMPs is only discussed in terms of adsorption, which affects the aggregation behaviour of PSMPs, and subsequent studies should be extended to more environmental behaviours such as aggregation and migration. For UV disinfection in wastewater treatment, there are also moments of simultaneous light exposure to EPS and PSMPs, so the interaction between phototransformed EPS and aged PSMPs should be investigated in order to have a comprehensive understanding of the environmental behaviour of EPS and microplastics.



## Consent to participate

All authors have given consent to their contribution.

## Consent for publication

All authors have agreed with the content and all have given explicit consent to publish.

## Author contributions

Shuyin Wei, investigation and original draft preparation; Feng Zeng, supervisor, funding support, writing review; Yingyue Zhou, sample collection; Jiawei Zhao, sample collection; Hao Wang, sample collection; Rui Gao, sample collection; Weiqian Liang, corresponding author, writing review.

## Conflicts of interest

The authors declare there is no conflicts of interest regarding the publication of this paper.

## Acknowledgements

This work was supported by the Natural Science Foundation of China (No. 41877462).

## References

- X. Huangfu, Y. Xu, C. Liu, Q. He, J. Ma, C. Ma and R. Huang, *Chemosphere*, 2019, **219**, 766–783.
- H.-C. Flemming and J. Wingender, *Water Sci. Technol.*, 2001, **43**, 9–16.
- Z. Ding, I. Bourven, G. Guibaud, E. D. van Hullebusch, A. Panico, F. Pirozzi and G. Esposito, *Appl. Microbiol. Biotechnol.*, 2015, **99**, 9883–9905.
- E.-M. Drakou, C. L. Amorim, P. M. Castro, F. Panagiotou and I. Vyrides, *Waste Biomass Valorization*, 2018, **9**, 2557–2564.
- Y. Shi, J. Huang, G. Zeng, Y. Gu, Y. Chen, Y. Hu, B. Tang, J. Zhou, Y. Yang and L. Shi, *Chemosphere*, 2017, **180**, 396–411.
- J. Teng, M. Wu, J. Chen, H. Lin and Y. He, *Chemosphere*, 2020, **255**, 126953.
- K. U. Mahto and S. Das, *Bioresour. Technol.*, 2022, **345**, 126476.
- S. He, L. Feng, W. Zhao, J. Li, Q. Zhao and L. Wei, *Chem. Eng. J.*, 2023, **462**, 142234.
- X. Liu, B. Ji and A. Li, *Water Res.*, 2023, **236**, 119960.
- C. Chen, T. Zhang, L. Lv, Y. Chen, W. Tang and S. Tang, *Water Res.*, 2021, **199**, 117161.
- A. D. Ren, G. P. Chen, J. H. Tang, P. Y. Zhang and S. G. Zhou, *Water Res.*, 2018, **134**, 54–62.
- H. Guo, S. Felz, Y. Lin, J. B. van Lier and M. de Kreuk, *Water Res.*, 2020, **181**, 115924.
- L. Xing, J. Yang, B.-J. Ni, C. Yang, C. Yuan and A. Li, *Sci. Total Environ.*, 2022, **811**, 152359.
- Y. Ahmed, J. Lu, Z. Yuan, P. L. Bond and J. Guo, *Water Res.*, 2020, **179**, 115878.
- S. Zhou, Z. Liao, B. Zhang, R. Hou, Y. Wang, S. Zhou, Y. Zhang, Z. J. Ren and Y. Yuan, *Environ. Sci. Technol.*, 2021, **55**, 15090–15099.
- T. Stanton, M. Johnson, P. Nathanail, W. MacNaughtan and R. L. D. Gomes, *Environ. Pollut.*, 2020, **263**, 114481.
- M. Wu, W. Tang, S. Wu, H. Liu and C. Yang, *Sci. Total Environ.*, 2021, **757**, 143902.
- T. Ye, A. Yang, Y. Wang, N. Song, P. Wang and H. Xu, *Environ. Pollut.*, 2022, **315**, 120354.
- P. Jachimowicz, Y.-J. Jo and A. Cydzik-Kwiatkowska, *Sci. Total Environ.*, 2022, **851**, 158208.
- J. Qian, X. He, P. Wang, B. Xu, K. Li, B. Lu, W. Jin and S. Tang, *Environ. Pollut.*, 2021, **279**, 116904.
- G.-Y. Zhen, X.-Q. Lu, Y.-Y. Li and Y.-C. Zhao, *Bioresour. Technol.*, 2013, **136**, 654–663.
- J. Ren, W. Fan, X. Wang, Q. Ma, X. Li, Z. Xu and C. Wei, *Water Res.*, 2017, **108**, 68–77.
- S. Comte, G. Guibaud and M. Baudu, *Enzyme Microb. Technol.*, 2006, **38**, 237–245.
- A. Maulana, R. S. Adiandri, R. Boopathy and T. Setiadi, *J. Biosci. Bioeng.*, 2022, **134**, 508–512.
- A. R. Badireddy, S. Chellam, P. L. Gassman, M. H. Engelhard, A. S. Lea and K. M. Rosso, *Water Res.*, 2010, **44**, 4505–4516.
- F. Freitas, V. D. Alves, J. Pais, N. Costa, C. Oliveira, L. Mafra, L. Hilliou, R. Oliveira and M. A. Reis, *Bioresour. Technol.*, 2009, **100**, 859–865.
- Z. Wang, Z. Wu and S. Tang, *Water Res.*, 2009, **43**, 2504–2512.
- S.-f. Yang and X.-y. Li, *Process Biochem.*, 2009, **44**, 91–96.
- W. Yan, W. Guo, L. Wang and C. Jing, *Sci. Total Environ.*, 2021, **784**, 147245.
- F. Hu, H. Zhai, Y. Yang, Y. Tian, J. Wang and H. Qiang, *J. Cleaner Prod.*, 2022, **367**, 133014.
- M. Hu, X. Wang, H. Wang, Y. Chai, Y. He and G. Song, *Luminescence*, 2012, **27**, 204–210.
- Z. Li, C. Wan, X. Liu, L. Wang and D.-J. Lee, *Sci. Total Environ.*, 2021, **756**, 144054.
- A. Abdurahman, K. Cui, J. Wu, S. Li, R. Gao, J. Dai, W. Liang and F. Zeng, *Ecotoxicol. Environ. Saf.*, 2020, **198**, 110658.
- L. Zhang, L. Luo and S. Zhang, *Colloids Surf., A*, 2012, **406**, 84–90.
- W. Chen, Z.-Y. Ouyang, C. Qian and H.-Q. Yu, *Environ. Pollut.*, 2018, **233**, 1–7.
- X. Zhang, S. Ma, B. Gao, F. Bi, Q. Liu, Q. Zhao, J. Xu, G. Lu, Y. Yang and M. Wu, *J. Colloid Interface Sci.*, 2023, **651**, 424–435.
- W. Chen, C. Qian, X.-Y. Liu and H.-Q. Yu, *Environ. Sci. Technol.*, 2014, **48**, 11119–11126.
- J. Ye, A. Hu, X. Cheng, W. Lin, X. Liu, S. Zhou and Z. He, *Water Res.*, 2018, **143**, 240–249.
- I. Noda and Y. Ozaki, *Two-Dimensional Correlation Spectroscopy: Applications in Vibrational and Optical Spectroscopy*, John Wiley & Sons, 2005.
- T. Ye, T. Fang, Y. Wang, S. Zhang, L. Bai, H. Xu, M. Guo and G. Sheng, *Environ. Res.*, 2021, **200**, 111424.
- R. Zafar, Z. Arshad, N. Eun Choi, X. Li and J. Hur, *Chem. Eng. J.*, 2023, **470**, 144031.

